ANNALS OF GEOPHYSICS, VOL. 49, N. 2/3, April/June 2006

Passive seismology in Southern Italy: the SAPTEX array

Giovanni Battista Cimini, Pasquale De Gori and Alberto Frepoli
Istituto Nazionale di Geofisica e Vulcanologia, Roma, Italy

Abstract
This paper describes the Southern APennines Tomography EXperiment (SAPTEX) temporary array deployed in Southern Italy from June 2001 to December 2004. Five to twelve three-components seismic stations, all equipped with RefTek 72A07 digitizers in continuous mode recording and Lennartz 3D/5 s sensors, were operating in the region during the four-year project. Many local, regional and teleseismic events have been recorded at 30 different recording sites, providing an invaluable data set for high-resolution seismological studies. Moreover, by the second half of 2002, some stations were installed in the Aeolian Islands with the main objective to record and better constrain the spatial distribution of the deep seismicity of the Southern Tyrrhenian subduction zone. The preliminary analysis of the waveforms collected in the first two years includes phase identification and body wave arrival time estimation, local earthquakes (re)location and focal mechanisms computation, *P*-wave traveltime residuals, and resolution of crustal and upper mantle structure derived by teleseismic ray sampling.

Key words *passive seismology – temporary array – crustal and upper mantle structure*

1. Introduction

In recent years the deployment of temporary passive arrays has contributed to improve our knowledge of the structure of the Earth's interior significantly. In Italy, linear arrays of ten to fifteen mobile stations have been deployed across the Apennines in the framework of the GeoModAp project (Amato *et al.*, 1998). For these experiments, the first of this kind ever carried out in Italy, seismometers were deployed for 3-4 months during the summers of 1994, 1995, and 1996 along three ~250-km-long lines from the Tyrrhenian Sea to the Adriatic Sea. The 1994 transect was installed in the Northern Apennines from Corsica to Mt. Conero. The 1995 transect was deployed in the Central Apennines from the Tyrrhenian coast north of Rome to the Tremiti Islands in the Adriatic Sea. Finally, the 1996 transect crossed the Southern Apennines from the Cilento to the Apulian region. The GeoModAp temporary arrays were carried out to collect new data for refining the existing tomographic models, studying the anisotropy in the crust and upper mantle, and inferring the Moho geometry through teleseismic receiver function analysis (Margheriti *et al.*, 1996; Ciaccio *et al.*, 1998).

The SAPTEX array was planned with the main goal to better resolve the crustal and upper mantle structure beneath Southern Italy. In this region the paucity of permanent seismic stations is still remarkable, thus preventing high-resolution tomographic studies, precise hypo-central determination, and detailed definition of the lithosphere-asthenosphere structure. Focusing on these objectives we proposed a long-term (at least two years), passive experiment with instruments capable of recording weak signals, such as teleseismic waveforms, as well as high-dynamic range signals from local and regional earth-

Mailing address: Dr. Giovanni Battista Cimini, Istituto Nazionale di Geofisica e Vulcanologia, Via di Vigna Murata 605, 00143 Roma, Italy; e-mail: cimini@ingv.it

quakes. The collection of a more complete and evenly distributed, high-quality data set is particularly important for reducing the uniqueness and resolution problems encountered when imaging the deep structure of the region. Recent tomographic studies have shown that this structure is rather complex, especially in the uppermost mantle where a possible along-strike discontinuity in the inferred Apenninic subduction has been detected (Amato *et al.*, 1993; Lucente *et al.*, 1999; Cimini and De Gori, 2001; Cimini, 2004). Indeed, between approximately 40°N and 42°N, the clear high-velocity anomalies delineating the subducted lithosphere beneath the Northern Apennines, to the north, and the Southern Tyrrhenian subduction zone, to the south, become weaker or even disappear in the first ~200 km. The seismic structure is furtherly complicated by the presence of pronounced low-velocity zones, reconstructed below the Central-Southern Apennines and the adjacent pery-Tyrrhenian area from the Moho down to at least 150 km depth. They indicate hot, probably partially melted, asthenospheric material in front of the Adriatic slab. As proposed by Cimini and De Gori (2001) and Cimini (2004), this asthenospheric upwelling might have promoted a faster termal assimilation of the downgoing continental lithosphere. The configuration of the SAPTEX passive array is potentially suitable for a high-definition mapping of the transition from the oceanic subduction beneath Calabria and Southern Tyrrhenian Sea to the complex continental collision/subduction in the Southern Apennines.

2. The temporary array

Figure 1 shows the distribution of the recording sites occupied by the SAPTEX array (circles) and the National Centralized Seismic Network (RSNC, squares) in Southern Italy. The deploy-

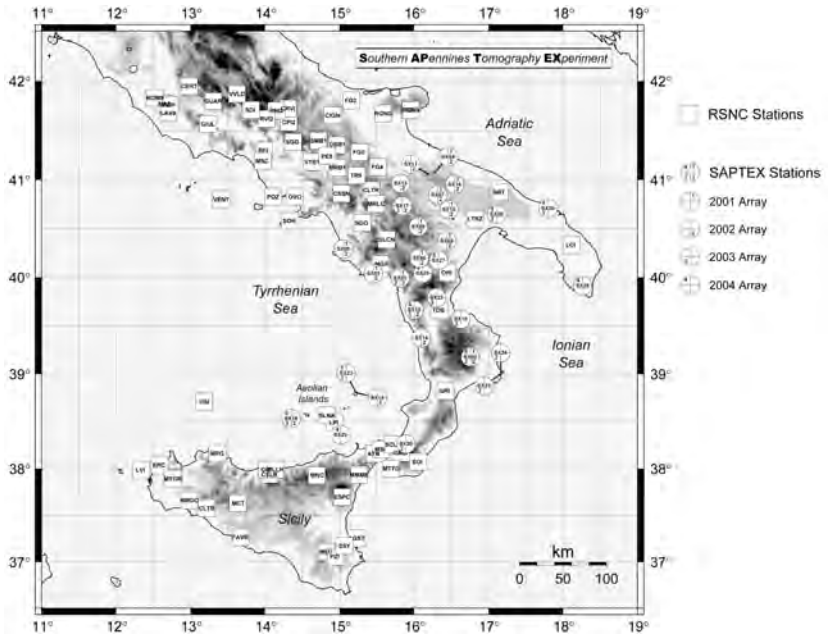

Fig. 1. Locations of the permanent and temporary seismic stations operating in Southern Italy in the period June 2001-December 2004. White squares are the permanent, mostly short-period, stations of the Istituto Nazionale di Geofisica e Vulcanologia (INGV) seismic network (RSNC). Circles are the temporary three-component stations deployed for the SAPTEX passive array during 2001 (1), 2002 (2), 2003 (3), and 2004 (4).

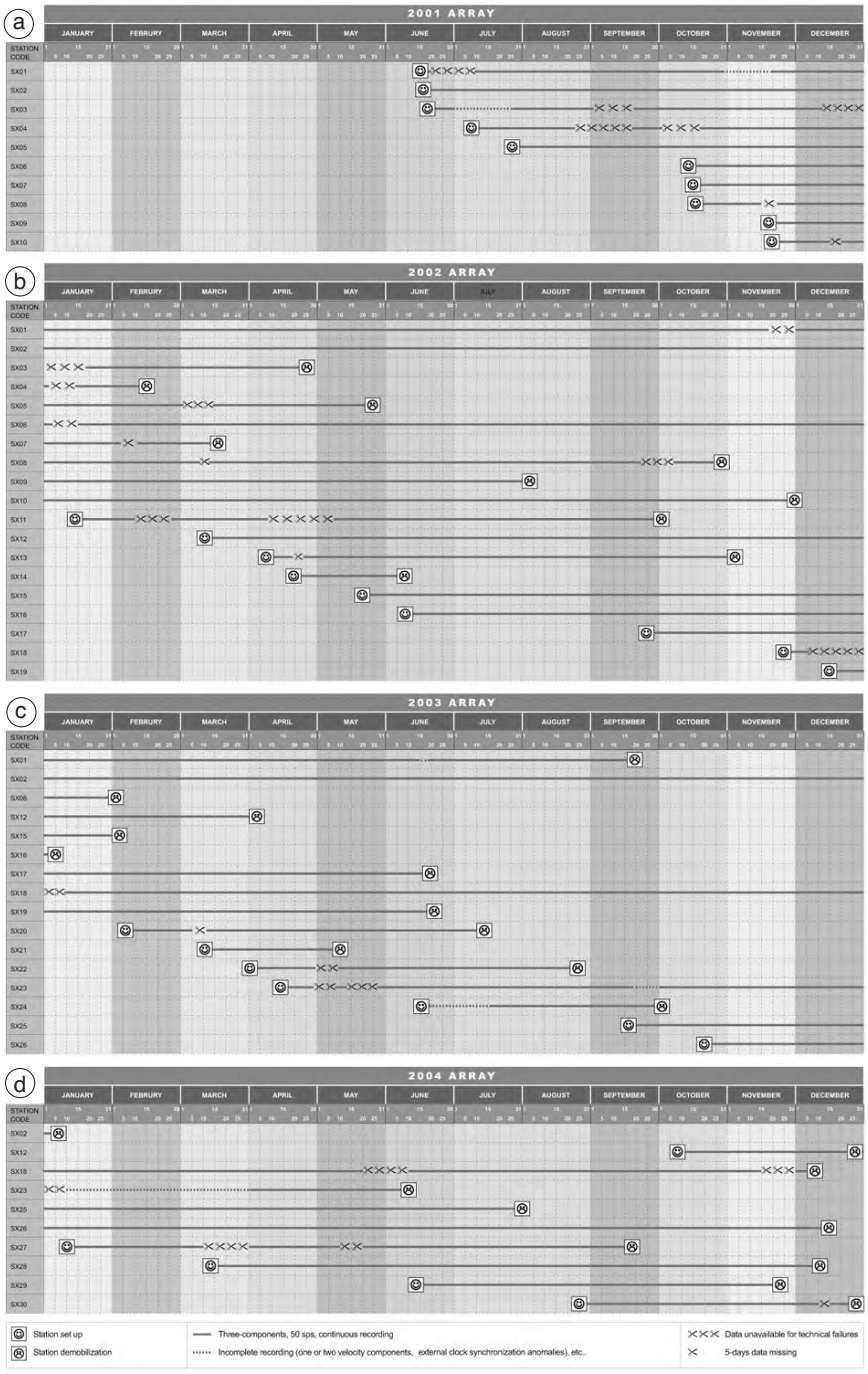

Fig. 2a-d. Operating history of the temporary stations during the four-year deployment (a-d). Station SX02 located in Central Calabria has operated continuously from June 20, 2001 to January 7, 2004 (932 days).

ment of the portable digital seismographs started at the end of June 2001. The first ten temporary stations (the 2001 array) were placed mostly in the Apulia and Basilicata regions, with the aim to reduce the large instrument spacing (~70 km) among the permanent existing stations. During 2002, nine new recording sites were added to increase the station coverage. Two stations of the 2002 array, SX15 and SX18, were in the Aeolian volcanic archipelago, on the Stromboli and Alicudi Island, respectively. These locations, although quite noisy (see fig. 4), were chosen to better constrain the hypocentral determination of the intermediate and deep seismicity characterizing the Tyrrhenian slab (Frepoli *et al.*, 1996). The geometry of the passive array has been furtherly improved by the 2003 and 2004 field programs that included eleven subsequent recording sites mainly located in Calabria, Aeolian Islands, and in the southern part of Apulia (fig. 1). The operating history tables shown in fig. 2a-d report details on the recording time interval and performance of the temporary stations in the data collecting period.

For each station we installed a 24 bit RefTek 72A07 digitizer, a three-components Lennartz 3D-5 s sensor (LE-3D/5s) with natural frequency and damping of 0.2 Hz and 0.70, respectively, a hard disk with capacity of 1, 2 or 4 Gb, two 70 Ah-12 V batteries, and two 45-Watt solar panels in sites where electrical power was unavailable. A GPS antenna provided the absolute timing for the recording. Digitizers were set to operate in continuous mode recording, with unitary preamplifier gain and sampling rate of 50 sps to record both teleseisms and local/regional seismicity. For the output, we adopted record lengths of 3600 s (hourly files) and compressed data format, which required changing the 1-Gb hard disks about once a month at the noisiest stations (*e.g.*, volcanic sites). At 50 sps, the amount of uncompressed raw data produced by each station is about 52 Mb/day. Figure 3 shows the station site and some components of the portable instrumentation installed at SX08, in the Southern Apennines (see table I for the location).

The frequency response of the LE-3D/5 s extended band sensors (velocity response flat from

Fig. 3. Photographs showing the station site SX08 (Pietrapertosa) located about 25 km SW the city of Potenza.

Table I. Description of the SAPTEX sites.

Station code	Site	Latitude (N)	Longitude (E)	Elevation (m)	Geology
SX01	Castrocucco	39.99380	15.81556	665	Calcarenite
SX02	Timpagrande	39.17936	16.75829	810	Granite
SX03	S. Giovanni a Piro	40.04109	15.45744	585	Calcarenite
SX04	Castel del Monte	41.07758	16.27273	529	Limestone
SX05	Rocca Cilento	40.29556	15.05511	682	Conglomerate

Table I (*continued*)**.**

Station code	Site	Latitude (N)	Longitude (E)	Elevation (m)	Geology
SX06	S. Chirico Raparo	40.19924	16.07590	968	Sandstone and marl
SX07	Barisci	40.84924	16.32098	469	Conglomerate
SX08	Pietrapertosa	40.52148	16.06124	1077	Feldspatic sandstone
SX09	Craco	40.37643	16.44330	367	Clay
SX10	Picciano	40.69913	16.47064	481	Clay and marl
SX11	Minevino Murge	41.06109	16.19586	598	Limestone
SX12	S. Sosti	39.66635	16.00190	588	Dolomitic limestone
SX13	Venosa	40.96438	15.82344	460	Conglomerate
SX14	Montalto Uffugo	39.37976	16.10046	990	Schist
SX15	Stromboli-S. Vincenzo	38.80264	15.23423	125	Basaltic lava
SX16	Quasano	40.95423	16.54832	520	Limestone
SX17	Pietragalla	40.73605	15.84764	870	Marl
SX18	Alicudi	38.53381	14.35637	156	Basaltic lava
SX19	Rossano	39.57064	16.63017	433	Phyllite
SX20	Celeste	38.26031	15.89393	694	Amphibolitic schist
SX21	Isola Capo Rizzuto	38.99696	17.15433	152	Sandstone
SX22	Cassano allo Jonio	39.78891	16.30720	473	Dolomitic limestone
SX23	Stromboli-P. Labronzo	38.80988	15.21803	165	Basaltic lava
SX24	Crotone	39.01600	17.16438	166	Sandstone
SX25	Massafra	40.64908	17.11090	431	Limestone
SX26	Carovigno	40.71468	17.79966	43	Limestone
SX27	Senise	40.17409	16.36029	298	Clay
SX28	Specchia	39.94845	18.27091	203	Limestone
SX29	Vulcano	38.39664	14.96412	159	Basaltic lava
SX30	San Severino Lucano	40.01356	16.14173	924	Conglomerate

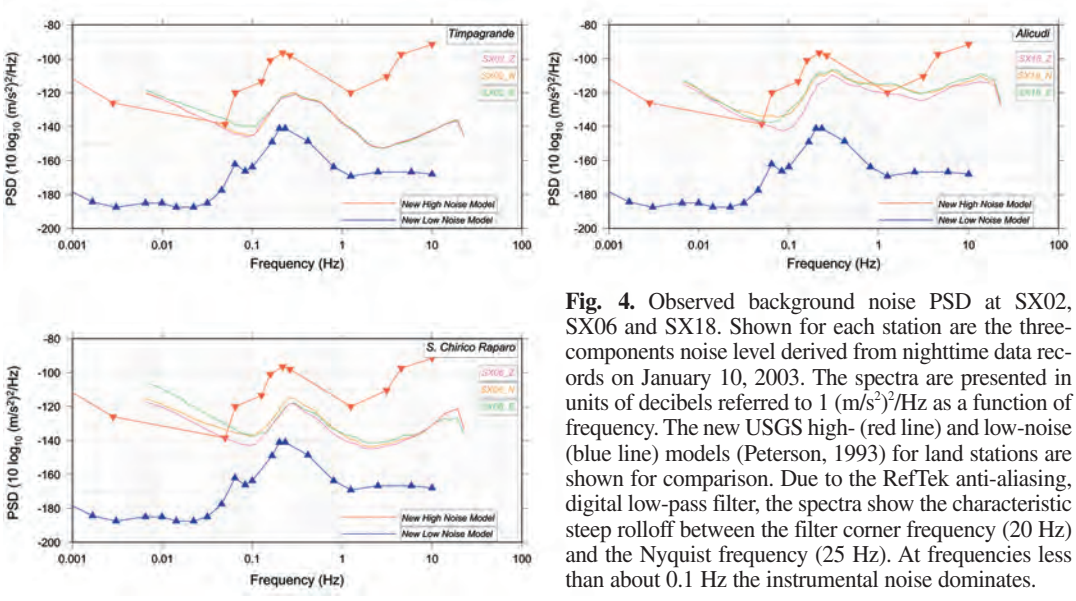

Fig. 4. Observed background noise PSD at SX02, SX06 and SX18. Shown for each station are the three-components noise level derived from nighttime data records on January 10, 2003. The spectra are presented in units of decibels referred to 1 $(m/s^2)^2/Hz$ as a function of frequency. The new USGS high- (red line) and low-noise (blue line) models (Peterson, 1993) for land stations are shown for comparison. Due to the RefTek anti-aliasing, digital low-pass filter, the spectra show the characteristic steep rolloff between the filter corner frequency (20 Hz) and the Nyquist frequency (25 Hz). At frequencies less than about 0.1 Hz the instrumental noise dominates.

0.2 to 40 Hz, decaying with 40 db/decade below the natural frequency) and the chosen sampling rate of 50 sps allowed the recording of weak ground motions in the frequency band between about 0.1 and 20 Hz. In this band, the main sources of seismic noise are the sea (marine microseismic band 0.05-1 Hz), the wind, cultural noise, and the site tectonics. Noise spectra for the SAPTEX stations were estimated by averaging the Power Spectral Densities (PSD) of 36, 100 s-long, ground acceleration samples. In order to have a smoother spectral estimate, each PSD was computed as mean value over geometrically spaced frequency (Cimini *et al.*, 1995). This smoothing method preserves the integral of the power spectrum. The spectral amplitudes were corrected for the instrumental response. Figure 4 displays the PSD estimates for the quietest (SX02), a good (SX06), and a noisy (SX18) station of the SAPTEX array. At station SX02, the high frequency noise level is close to the expected instrumental noise. The noise level at SX18, located on the westernmost island of the Aeolian archipelago (fig. 1), is affected by both the nearness of the sea and the volcanic setting.

3. Waveform analysis and preliminary results

The following subsections show examples of seismogram analysis and some initial results obtained by merging the data collected by the SAPTEX array during the first two years of deployment with the data recorded in the same period by the permanent stations of the RSNC located in Central-Southern Italy (fig. 1).

3.1. *Example of seismograms*

Figure 5 shows the seismograms of the October 31, 2002 Molise earthquake recorded at the closest operating station of the SAPTEX array. Station SX13, near the city of Venosa, was located about 111 km SE (backazimuth 316°) from the epicentral area. At this distance, the crustal

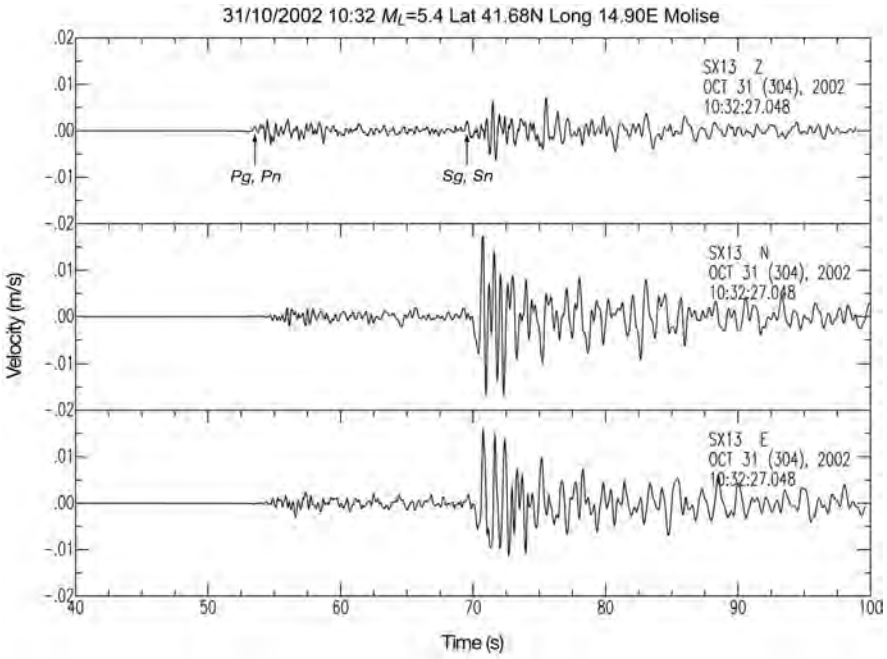

Fig. 5. Three-components ground velocity recording of the October 31, 2002 Molise earthquake at SX13.

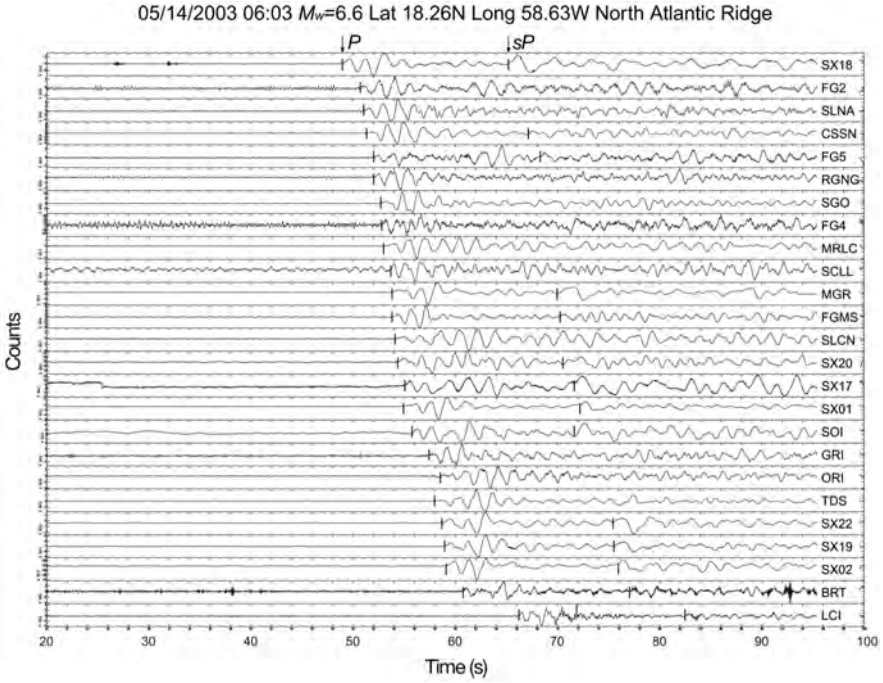

Fig. 6. Unfiltered seismograms (vertical components) of a teleseismic event (*P* phases) that occurred in the region of North Atlantic ridge (epicentral distance =53°, backazimuth =270°, depth =42 km). The first breaks on *P* and *sP* arrivals are marked with the vertical bars. The Earth's surface reflected phase *sP* is observed, more clearly on the SAPTEX recordings, after about 17 s.

structure of the ak135 velocity model (Kennett *et al.*, 1995) predicts *Pg*, *Pn* and *Sg*, *Sn* phases with very similar arrival times, as indicated on the plot. The M_L 5.4 Molise earthquake was the strongest event that occurred in the Southern Apennines during the experiment. The most important local events that occurred within the temporary network were the April 13, 2002 M_d 3.3 and the April 18, 2002 M_d 4.1 earthquakes, both located in the Basilicata region. A complete study of the diffuse, low-magnitude seismicity recorded in this region and adjacent areas in the last five years is currently in progress. The results obtained by analizing the local earthquake data for the period 2001-2002 are discussed in Frepoli *et al.* (2005) and, for some selected events, are presented in Section 3.2.

The continuous recordings have been carefully examined also for phase identification and arrival time picking of regional ($3°<\Delta<15°$) and telesesimic ($\Delta>30°$) events. The digital waveforms of over 5000 *Pn* and *Sn* phases were collected from events with magnitude $M\geq4.0$ located all around the Mediterranean Sea. With these data we expect to provide insight into the lithospheric mantle structure through *Pn* velocity and Sn attenuation tomography studies. For the teleseismic tomography component of the project we have selected so far 214 $M_w\geq5.5$ earthquakes distributed around the globe. Source backazimuths are primarily from the northeast quadrant and west directions, with a few events arriving from the south. Figure 6 shows the seismograms of a North Atlantic ridge event recorded at 25 stations of the integrated network. The *P*-wave arrival times were estimated by visually correlating the waveforms in the early part of each seismic trace (the first two-three cycles) and picking the first break of the wave train. Special attention was paid to the reading of core phases *PKPdf*,

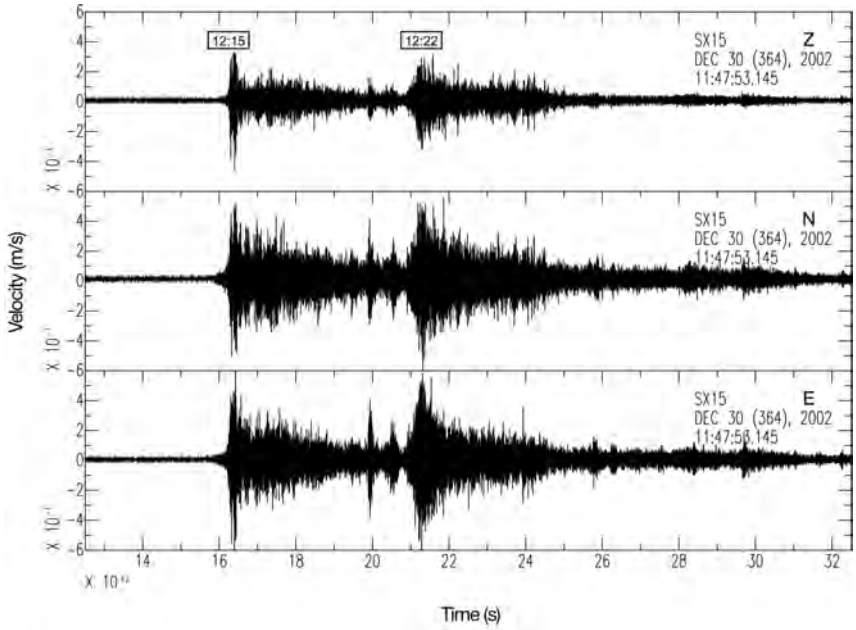

Fig. 7. Seismograms of the December 30, 2002 slump episodes that occurred at Stromboli Volcano in the Sciara del Fuoco area, on the northwestern side. The landslides were recorded at station SX15 installed at the INGV-San Vincenzo Observatory.

most often made difficult by the close arrivals of the more energetic *PKPbc* or *PKPab* phases, and of later arriving phases such as *pP* and *sP* from deep earthquakes and core reflected *PcP*. This analysis yielded a set of 5859 picks of first arrivals (*P* and *PKPdf*), and 569 picks of later arrivals (*pP*, *sP*, *PcP*, *PKPbc*, etc.). Although these secondary phases are not as easy to identify as first arrivals, they are worth searching for. Already a limited number of them can greatly improve the ray coverage within the target volume, reducing the incidence-angle gap between direct rays (Cimini and De Gori, 1997).

Finally, fig. 7 displays the seismic signals produced by the landslides that occurred at Stromboli volcano, Aeolian Islands (fig. 1), on December 30, 2002, recorded by station SX15. This location was very fortunate being in the near field only ~2 km from the Sciara del Fuoco area where the events took place. The ground velocity seismograms show two main high frequency episodes, about 500 s from each other, characterized by similar aspect and duration (~300 s). Other trains of pulses with shorter duration and lower amplitude are recognizable in the coda of the main event, possibly indicating the occurrence of minor, further mass detachment episodes. On the basis of a waveform modeling study recently carried out (Pino *et al.*, 2004), the first event has been interpreted as due to a submarine slump, associated with the observed tsunami, while the second would represent the signal of the following subaerial landslide.

3.2. *Relocation and focal mechanisms computation of some Southern Apennines earthquakes*

In order to estimate the improvement in the location and in the focal mechanisms computation of earthquakes in Southern Italy using the additional data from the SAPTEX passive array, we selected three events that occurred in the Basili-

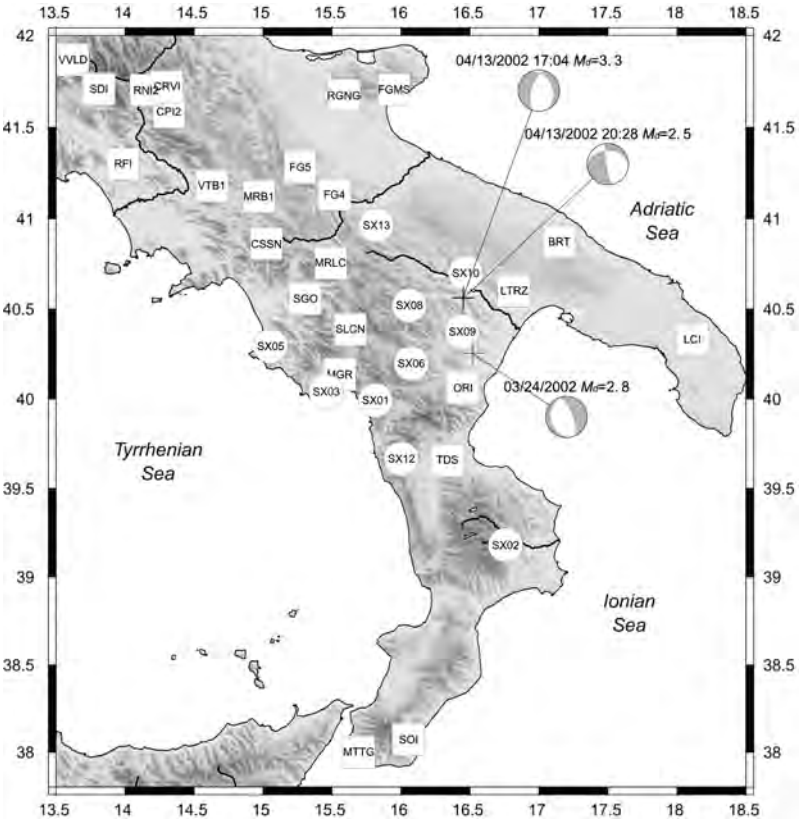

Fig. 8. Map showing location and focal mechanisms for three Southern Apennines earthquakes. Also displayed are the RSNC and SAPTEX seismic stations used for the analysis.

Table II. Layered velocity model and *Vp*/*Vs* ratio adopted for location and focal mechanism computation.

Velocity (km s^{-1})	Top of layer (km)
4.5	0.0
5.7	6.0
6.5	10.0
8.1	30.0
Vp/*Vs*	1.80

cata region: the March 24, 2002, M_d 2.8 (00:11 UTC), located in the lower Agri valley, the April 13, 2002, M_d 3.3 (17:04 UTC), and the M_d 2.5 (20:28 UTC), both located in the middle Basento valley. All three events were recorded by both the RSNC and the SAPTEX networks (fig. 8). For the hypocentral relocations we used the computer program HYPOINVERSE (Klein, 1989), and the Amato and Selvaggi (1993) 1D velocity model with a *Vp*/*Vs* ratio of 1.80 (table II). This value was selected in the range 1.75÷1.82 testing the location errors. The fault plane solutions were computed using the FPFIT code (Reasenberg and Oppenheimer, 1985).

The hypocentral parameters determined for the selected events by using only RSNC data and with both RSNC and SAPTEX data are shown in tables III and IV, respectively. The horizontal and vertical errors (ERH and ERZ) are simplified errors derived from the lengths and directions of the principal axes of the error ellipsoid. Reloca-

Table III. Hypocentral parameters, magnitude, azimuthal gap, number of *P* and *S* readings, rms, and location errors for three Southern Apennines events computed using data only from the permanent stations of the RSNC network.

Date	Ot	Lat	Long	Depth	M_d	Gap	Nph	Rms	ERH	ERZ
24/03/2002	00:11:02.58	40°13.92	16°30.65	39.6	2.8	157	7	0.18	1.4	9.3
13/04/2002	17:04:47.70	40°35.00	16°24.08	14.1	3.3	78	20	0.38	0.9	1.7
13/04/2002	20:28:08.25	40°34.16	16°24.78	22.7	2.5	136	7	0.32	1.6	6.4

Table IV. The same as in table III with the computation performed by using data from both the permanent stations and the temporary stations of the SAPTEX array.

Date	Ot	Lat	Long	Depth	M_d	Gap	Nph	Rms	ERH	ERZ
24/03/2002	00:11:02.27	40°14.59	16°32.17	47.4	2.8	159	20	0.34	1.3	1.8
13/04/2002	17:04:47.74	40°33.94	16°26.13	24.0	3.3	96	28	0.41	0.8	0.6
13/04/2002	20:28:08.07	40°33.71	16°28.09	27.3	2.5	101	21	0.32	1.3	0.5

tions with only RSNC data show ERH smaller than 1.6 km, while ERZ are quite a bit larger, ranging between 1.7 and 9.3 km (table III). Generally, using only the RSNC data, the hypocentral depth shows the largest uncertainty among the hypocentral parameters. This is due to the large spacing between the RSNC stations, which is about 70 km in the area. Root-mean-square travel time residuals (rms) are equal or smaller than 0.38s for all three earthquakes. The largest azimuthal gap in the relocation is smaller than 157° for all three events and the hypocentral depths range between 14 and 40 km (table III). We observe a large improvement in the depth determination when using both RSNC and SAPTEX arrival times. In these relocations, ERH and ERZ are smaller than 1.3 km and 1.8 km, respectively, for all three events (table IV). The March, 24, 2002 earthquake is a subcrustal event with depth around 47 km.

We computed fault plane solutions for all three events relocated with both datasets (fig. 9a-c; table VI). Using the RSNC data, it was only possible to determine a focal mechanism for the April 13, 2002, 17:04 event due to the large number of polarities available (fig. 9b1 and table V). This solution shows a large strike-slip component with *T*-axes W-NW oriented. The fault plane solution of the deepest earthquake (March 24, 2002) relocated with both data sets shows a pure normal solution with minimum compression axes oriented E-NE (fig. 9a). The April 13, 2002 *M* 3.3 event relocated with both datasets (fig. 9b2; fig. 10) shows a focal mechanism quite different from that computed with only the RSNC polarities. This normal solution is more constrained due to inclusion of the SAPTEX polarities. It shows a small strike-slip component and *T*-axes E-W oriented. The fault plane solution for the second Basentano event computed with both RSNC and SAPTEX data shows a normal solution with NE-SW *T*-axes (fig. 9c).

The quality of fault plane solution is given by two output quality factors (*Qf* and *Qp*) of the FPFIT code (Reasenberg and Oppenheimer, 1985). *Qf* reflects the solution prediction misfit to the polarity data *Fj* (*Fj*=0.0 represents a perfect fit to the data, while *Fj*=1.0 represents a perfect misfit). *Qp* summarizes the three parameter uncertainties Δs, Δd and Δr (ranges of perturbations to strike, dip and rake, respectively). Quality decreasing values are indicated with A, B and C (table VII). All solutions with one or both quality factors equal to C were rejected. Quality factors of the selected focal mechanisms are shown in table VI. Only the April 13, 2002 M_d 3.3 event shows one discrepant observation (*Qf*=B).

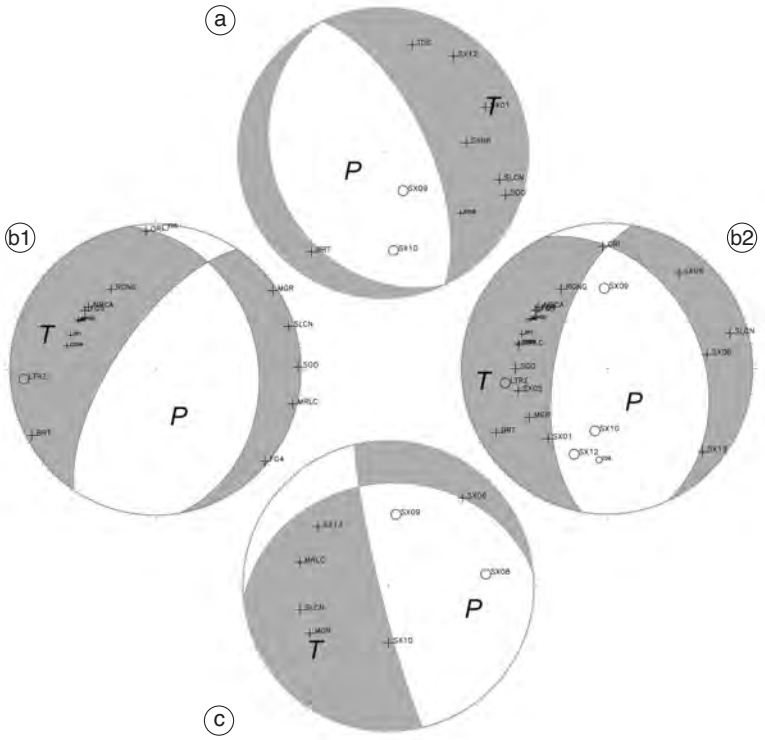

Fig. 9a-c. Fault-plane solutions of the three selected events located in the Southern Apennines: a) 24/3/2002, 00:11; b1-b2) 13/04/2002, 17:04; c) 13/04/2002, 20:28. Focal mechanism (b1) is computed with only the RSNC data, while a), b2) and c) are computed with both RSNC and SAPTEX data.

Table V. Strike, dip, rake and quality factors of the April 13, 2002, 17:04 event fault plane solution computed with RSNC data.

Event	Strike	Dip	Rake	*Qf*	*Qp*
13/04/2002 17:04	350	30	−130	B	B

Table VI. Strike, dip, rake and quality factors of the fault plane solutions computed with both RSNC and SAPTEX data.

Event	Strike	Dip	Rake	*Qf*	*Qp*
24/03/2002 00:11	155	25	−90	A	A
13/04/2002 17:04	335	35	−120	B	A
13/04/2002 20:28	265	30	−170	A	B

The large hypocentral depths found for these Basentano events are similar to those observed for the May 1990 Potenza seismic sequence (Azzara *et al.*, 1993). This sequence was localized about 30 km to the WNW from the middle Basento valley events and shows hypocentral depths ranging from 15 to 25 km. We believe that the large observed depths are a distinctive feature of the seismicity in this part of the Southern Apennines.

3.3. *Resolution of tomographic models of the deep structure beneath Southern Italy*

To investigate the depth resolution of tomographic models of the upper mantle beneath the SAPTEX array we have performed a resolution

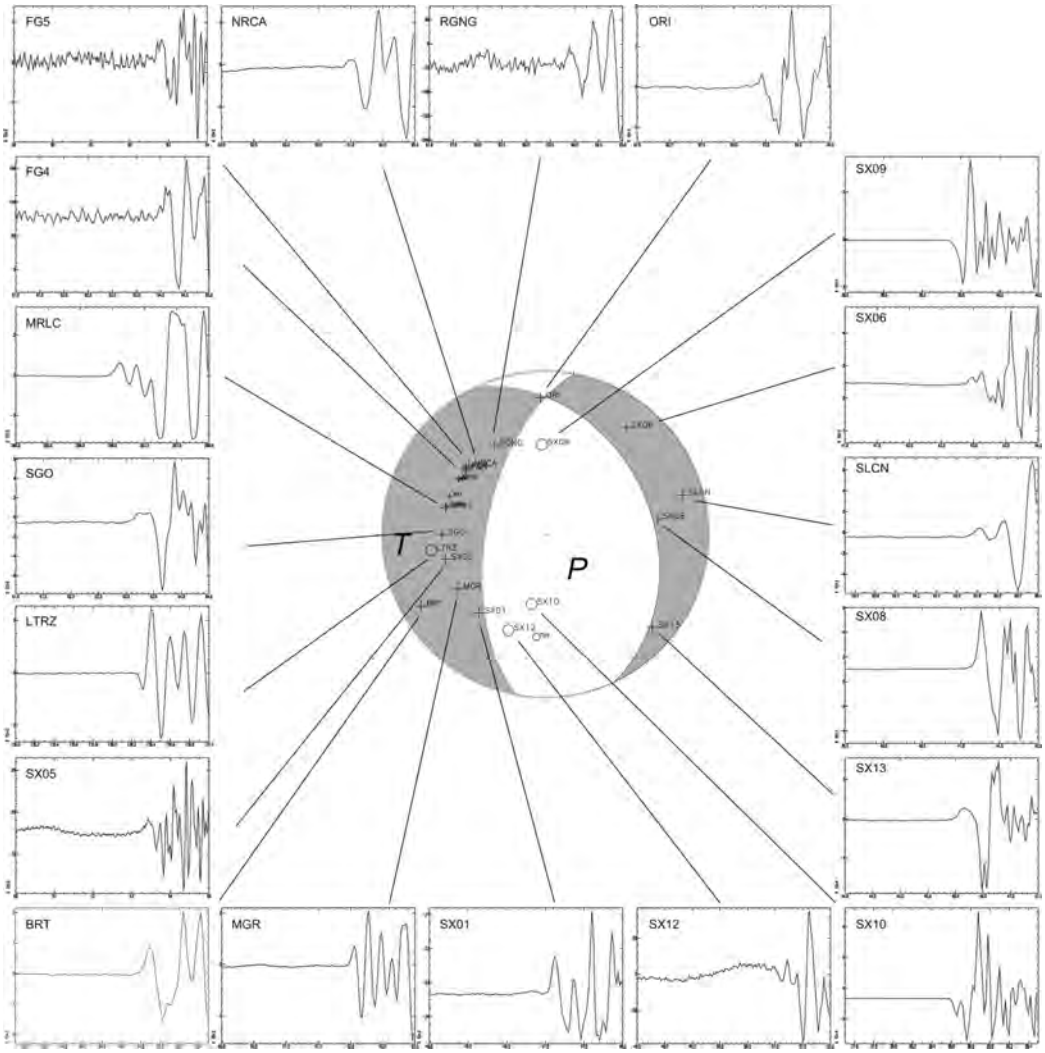

Fig. 10. Fault-plane solution and waveforms showing polarities of the *P*-wave arrivals of the April, 13, 2002 event.

Table VII. Fault plane solution quality factors *Qf* and *Qp*. *Fj* is the solution prediction misfit to the polarity data; Δstr, Δdip, Δrake are ranges of variability of strike, dip and rake, respectively.

	Qf		*Qp*
A	$Fj \leq 0.025$	A	Δstr, Δdip, Δrake ≤ 20°
B	$0.025 < Fj \leq 0.1$	B	20° to 40°
C	$Fj > 0.1$	C	>40°

test using the distribution of paths of teleseismic *P* and *PKPdf* waves recorded during the first two years of the field experiment. The *P*-wave path set consists of 5859 rays (4087 *P* and 1772 *PKPdf*) associated with the event-station pairs of 214 teleseisms recorded by both the RSNC network and the SAPTEX temporary array. Figure 11 shows the great circle paths of this data set. The SAPTEX recordings (green paths) con-

tribute to enhancing the sampling of the deep structure under the study area. Figure 12 shows the relative traveltime residuals observed at SX02, the most representative station of the passive array (figs. 2 and 4), as a function of back-azimuth and epicentral distance of the teleseismic events. They were computed with respect to the 1D ak135 (Kennett *et al.*, 1995) velocity model after correction of the *P*-wave arrival times for Earth's ellipticity and station elevation.

The resolution analysis was carried out by computing the model resolution matrix for a weighted damped least squares solution of the inverse problem relating the observed teleseismic travel times to the velocity deviations within the target volume. To trace ray paths needed to form the kernel matrix and to compute theoretical travel times needed to determine the arrival times delays, the target volume was parameterized by using a 3D grid of nodes with preassigned *P*-wave velocity based on the ak135 model. The 3D grid consisted of 96 station nodes and ten layers of nodes, each consisting of a 2D mesh of 19×19 nodes, having lateral spacing ranging from 35×35 km (layer 1) to 80×80 km (layer 10). The layer depths below the surface were chosen at 30, 65, 105, 150, 200, 260, 330, 410, 500, and 600 km. For the inversion we used a modern teleseismic tomography procedure based on the Singular Value Decomposition (SVD) method which, at some computational expense, circumvents approxi-

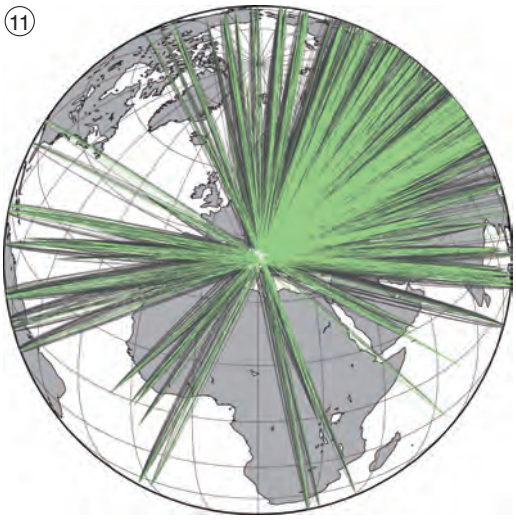

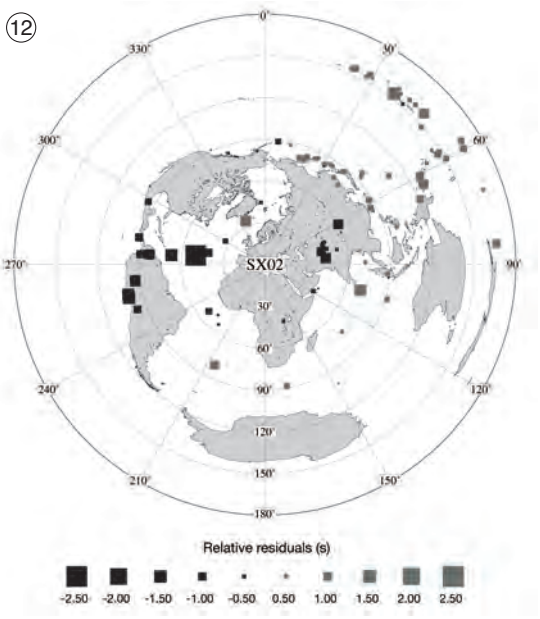

Fig. 11. Orthographic map (projection center at 39.5N-15.0E) showing the ray trajectories (great circle paths) of the *P* and *PKPdf* phases recorded during the period June 2000-June 2003. White circles are the seismic stations of fig. 1. The events are distributed over a wide range of back azimuths, although the majority of them are located between back azimuths of 330° and 120°. The additional raypaths provided by the SAPTEX recordings (green raypaths) improve the ray sampling of the deep structure beneath the study region significantly.

Fig. 12. *P*-wave travel time residuals from teleseismic events recorded at station SX02. The pattern displays a strong directional dependence of relative residuals. Negative residuals, as large as −2.5 s, are observed for rays approaching the station from western directions, whereas positive values are predominant for events incoming from the NE quadrant. This pattern is consistent with the uppermost mantle *P*-wave velocity structure delineated by recent nonlinear traveltime inversions (Cimini, 1999; Cimini and De Gori, 2001).

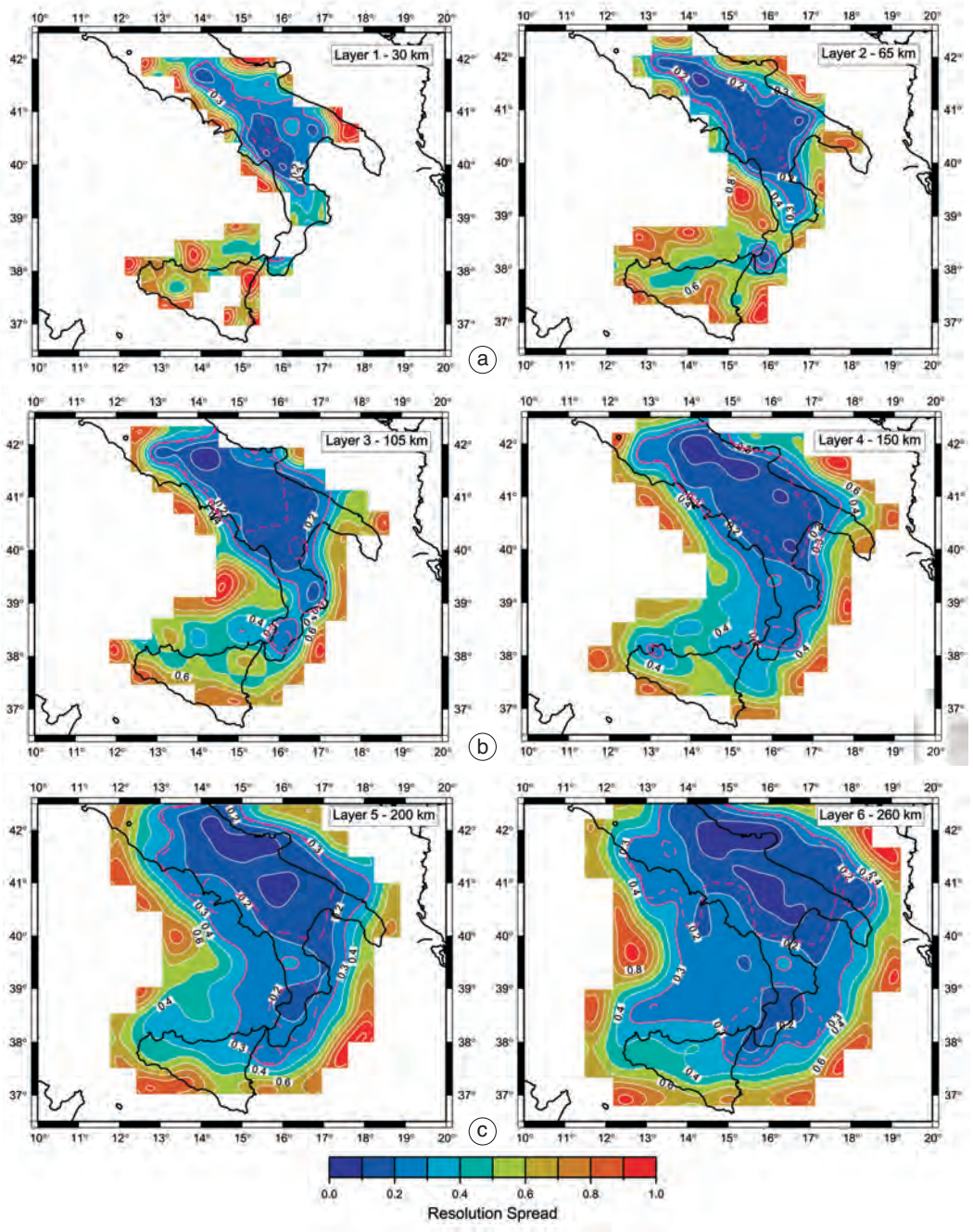

Fig. 13a-c. Map views of resolution spread for the lower crust and uppermost mantle of Southern Italy displaying how well the seismic structure would be resolved by the ray sampling of fig. 11. Nodes within the blue regions (resolution spread <0.4) correspond to well-resolved model parameters. Nodes with larger resolution spread indicate estimates of model parameters that are really weighted averages of the true model parameters. See text for further details.

mate techniques and allows one to obtain a direct estimate of the model resolution (Cimini, 1999; Cimini and De Gori, 2001). Using this approach we determined the resolution matrix for 1132 model parameters. Figure 13 shows the resolution spread computed for nodes lying on the first six layers of the starting model. The resolution spread is a simple but effective way to quantify the goodness of model resolution based on the size of the off-diagonal elements. In particular we adopted the measure based on the L_2 norm of the difference between the resolution matrix $\boldsymbol{R}$ and the identity matrix $\boldsymbol{I}$ (Menke, 1989). When $\boldsymbol{R}=\boldsymbol{I}$ the model parameters are uniquely determined (perfectly resolved) and spread($\boldsymbol{R}$)=0. In the layer maps of fig. 13, the magenta curve (the 0.3 contour) borders the well-resolved parts of the model. Nodes within these regions are characterized by negligible contribution of the off-diagonal elements associated with the neighbouring nodes, thus indicating limited smearing effects and volume averaging of the model parameters (velocity anomalies). For comparison, the dashed magenta curve contours the 0.3 level of the resolution spread pattern obtained by using only the RSNC teleseismic path set (the black paths in fig. 11). It is noteworthy the resolution improvement provided by the long-term deployment of the SAPTEX array especially in those areas, like Basilicata and Northern Calabria, where the transition from the Southern Tyrrhenian oceanic subduction to the Southern Apennines continental subduction makes the deep seismic structure very complex and still poorly understood (Cimini and De Gori, 2001; Cimini, 2004). This result is strongly encouraging and we believe that the dataset of the entire SAPTEX deployment will allow us to produce more reliable, high-resolution tomographic images of the mantle beneath the region.

4. Conclusive remarks

The SAPTEX passive array represents the longest deployment of portable seismic stations carried out in Italy. During the four-year project we recorded a large amount of data essential for gaining a clearer picture of the lithosphere-asthenosphere system beneath Southern Italy. The experiment produced ~500 Gb of raw data from which ~25 Gb of digital waveforms of local, regional and teleseismic events have been extracted. The initial results on the computation of hypocentral parameters and fault plane solutions of local earthquakes show the benefit of using data from the temporary stations. Particularly interesting is the new evidence on the occurrence of lower crust seismicity and, for the first time, the observation of a subcrustal event below Eastern Basilicata. The denser station coverage achieved with the experiment allowed us to greatly improve the ray sampling of the deep structure, making feasible the planned high-resolution imaging of the seismic velocity field. The SAPTEX dataset will provide an unprecedented opportunity also for studies concerning the reconstruction of the Moho geometry from receiver function analysis, seismic aniso-tropy, attenuation tomography, and seismotectonic.

Acknowledgements

We are grateful to A. Amato for his continuous encouragement and helpful advice. We thank M. Cattaneo, M. De Martinis, G. Colasanti, E. Giandomenico, M. Silvestri, and S. Silvestri for technical support during the field experiment. We also thank A. Marchetti for help in waveforms analysis and B. Angioni for help in drafting. The SAPTEX project was funded by the Centro Nazionale Terremoti (CNT) of the Istituto Nazionale di Geofisica e Vulcanologia (INGV).

REFERENCES

AMATO, A. and G. SELVAGGI (1993): Aftershock location and *P*-velocity structure in the epicentral region of the 1980 Irpinia earthquake, *Ann. Geofis.,* **XXXVI** (1), 3-25.

AMATO, A., B. ALESSANDRINI, G.B. CIMINI, A. FREPOLI and G. SELVAGGI (1993): Active and remnant subducted slabs beneath Italy: evidence from seismic tomography and seismicity, *Ann. Geofis.*, **XXXVI** (2), 201-214.

AMATO, A., L. MARGHERITI, R. AZZARA, A. BASILI, C. CHIARABBA, M.G. CIACCIO, G.B. CIMINI, M. DI BONA, A. FREPOLI, F.P. LUCENTE, C. NOSTRO and G. SELVAGGI (1998): Passive seismology and deep structure in Central Italy, *Pure Appl. Geophys*., **151**, 479-493.

AZZARA, R., A. BASILI, L. BERANZOLI, C. CHIARABBA, R. DI GIOVAMBATTISTA and G. SELVAGGI (1993): The seismic

sequence of Potenza (May 1990), *Ann. Geofis*., **XXXVI** (1), 237-243.

CIACCIO, M.G., G.B. CIMINI and A. AMATO (1998): Tomographic images of the upper mantle high-velocity anomaly beneath Northern Apennines, *Mem. Soc. Geol. It*., **52**, 353-364.

CIMINI, G.B. (1999): *P*-wave deep velocity structure of the Southern Tyrrhenian Subduction Zone from nonlinear teleseismic traveltime tomography, *Geophys. Res. Lett*., **26**, 3709-3712.

CIMINI, G.B. (2004): Tomographic studies of the deep structure of the Tyrrhenian – Apennine system, in *From Seafloor to Deep Mantle: Architecture of the Tyrrhenian Backarc Basin*, edited by M. MARANI, F. GAMBERI, and E. BONATTI, *Mem. Descr. Carta Geol. Ital.*, **XLIV**, 15-28.

CIMINI, G.B. and P. De GORI (1997): Upper mantle velocity structure benath Italy from direct and secondary *P*-wave teleseismic tomography, *Ann. Geofis.*, **XL** (1), 175-194.

CIMINI, G.B. and P. DE GORI (2001): Nonlinear *P*-wave tomography of subducted lithosphere beneath Central-Southern Apennines (Italy), *Geophys. Res. Lett*., **28**, 4387-4390.

CIMINI, G.B., A. AMATO, M. CERRONE, M. CHIAPPINI, M. DI BONA and S. PONDRELLI (1995): Passive seismological studies in the Terra Nova Bay area (Antarctica): first result from the 1993-1994 expedition, *Terra Antartica*, **2**, 81-94.

FREPOLI, A., G. SELVAGGI, C. CHIARABBA and A. AMATO (1996): State of stress in the Southern Tyrrhenian subduction zone from fault-plane solutions, *Geophys. J. Int*., **125**, 879-891.

FREPOLI, A., F.R. CINTI, L. AMICUCCI, G.B. CIMINI, P. DE GORI and S. PIERDOMINICI (2005): Pattern of seismicity and state of stress in the Lucanian Apennines foredeep (Southern Italy) from recording by the SAPTEX temporary array, *Ann. Geophysics*, **48** (6), 1035-1054.

KENNETT, B.L.N., E.R. ENGDHAL and R. BULAND (1995): Constraints on seismic velocities in the Earth from traveltimes, *Geophys. J. Int*., **126**, 555-578.

KLEIN, R.W. (1978): Hypocenter location program HYPOINVERSE, Part I. Users guide to version 1, 2, 3 and 4, *USGS Open-file Rep. 78-964*.

LUCENTE, F.P., C. CHIARABBA, G.B. CIMINI and D. GIARDINI (1999): Tomographic constraints on the geodynamic evolution of the Italian region, *J. Geophys. Res*., **104**, 20,307-20,327.

MARGHERITI, L., C. NOSTRO, M. COCCO and A. AMATO (1996): Seismic anisotropy beneath the Northern Apennines (Italy) and its tectonic implications, *Geophys. Res. Lett.,* **23**, 2721-2724.

MENKE, W. (1989): *Geophysical Data Analysis: Discrete Inverse Theory* (Academic Press, San Diego, California), pp. 260.

PETERSON, J. (1993): Observations and modeling of seismic background noise, *USGS Open-file Rep. 93-322*.

PINO, N.A., M. RIPEPE and G.B. CIMINI (2004): The Stromboli volcano landslides of December 2002: a seismological description, *Geophys. Res. Lett.,* **31**, L02605.

REASENBERG, P. and D. OPPENHEIMER (1985): FPFIT, FPPLOT and FPPAGE: FORTRAN computer programs for calculating and display ing earthquake fault-plane solutions, *USGS Open-file Rep. 85-739*.